Biomolecules & Biomedicine

RESEARCH ARTICLE

Pathologic complete response and residual disease after neoadjuvant chemotherapy in breast cancer: Comparison of contrast-enhanced mammography, DCE-MRI, and ^{18}F-FDG PET/CT

Ebru Ozan Sanhal[1], İmren Mutlu[1*], Evrim Sürer Budak[2], Veli Vural[3], İsmail Zihni[3], Kübra Simşek[4], Sema Sezgin Göksu[5], and Cumhur Arıcı[3]

Accurate assessment of breast cancer response to neoadjuvant chemotherapy (NAC) is important for surgical planning. We compared contrast-enhanced mammography (CEM), dynamic contrast-enhanced magnetic resonance imaging (DCE-MRI), and fluorine-18 fluorodeoxyglucose positron emission tomography/computed tomography (^{18}F-FDG PET/CT) for predicting breast pathologic complete response (pCR) and assessing residual disease. This retrospective single-center study included 76 patients who underwent all three modalities before and after NAC, followed by surgery. Postoperative histopathology was the reference standard; breast pCR was defined as the absence of residual invasive carcinoma in the breast, irrespective of residual ductal carcinoma in situ. Breast pCR occurred in 28 patients (36.8%). CEM had higher sensitivity than DCE-MRI (89.3% versus 60.7%; $P = 0.012$) and the highest negative predictive value (92.1%), whereas DCE-MRI had the highest specificity (85.4%) and positive predictive value (70.8%). Accuracy was 79.0%, 76.3%, and 73.7% for CEM, DCE-MRI, and ^{18}F-FDG PET/CT, respectively, without a significant difference among modalities ($P = 0.661$). Corresponding areas under the receiver operating characteristic curve were 0.841, 0.844, and 0.769. Among 48 patients with residual invasive disease, intraclass correlation coefficients for CEM and DCE-MRI measurements versus pathology were 0.733 and 0.773, respectively. However, 95% limits of agreement were wide (−34.16 to 25.16 mm and −29.26 to 20.93 mm, respectively), indicating substantial individual-level discrepancies. CEM showed promise for post-NAC breast response assessment in this selected cohort, but the findings do not establish equivalence or interchangeability with DCE-MRI. Individual tumor size estimates require caution, and prospective multicenter validation is warranted.

Keywords: Breast cancer, neoadjuvant chemotherapy, contrast-enhanced mammography, magnetic resonance imaging, ^{18}F-FDG PET/CT.

Introduction

Neoadjuvant chemotherapy (NAC) is a standard treatment for patients with locally advanced and inflammatory breast cancer. Its primary goals are to downstage the disease and facilitate breast-conserving surgery (BCS) [1–3]. Patients achieving a pathologic complete response (pCR) after NAC experience improved outcomes, including lower recurrence rates and better survival, compared to those with residual disease [4, 5]. Therefore, accurate preoperative response assessment is crucial to confirm therapeutic efficacy, identify poor responders who might benefit from treatment modification, and guide surgical planning.

Current guidelines recommend dynamic contrast-enhanced magnetic resonance imaging (DCE-MRI) as the most accurate imaging technique for preoperative staging and evaluating NAC response [6]. However, the routine use of DCE-MRI can be limited by availability, cost, examination time, and contraindications (e.g., certain implanted devices, severe claustrophobia, or gadolinium-related concerns). These limitations have spurred interest in alternative imaging approaches that could reliably assess residual disease and predict pCR.

Contrast-enhanced mammography (CEM) is a dual-energy technique performed after intravenous administration of iodinated contrast material. It provides low-energy (LE) images comparable to full-field digital mammography and recombined images (RC) that highlight contrast enhancement related to tumor vascularity [7, 8]. Previous studies have demonstrated that CEM improves breast cancer detection compared to

[1]Department of Radiology, Akdeniz University Faculty of Medicine, Antalya, Türkiye; [2]Department of Nuclear Medicine, Akdeniz University Faculty of Medicine, Antalya, Türkiye; [3]Department of General Surgery, Akdeniz University Faculty of Medicine, Antalya, Türkiye; [4]Department of Pathology, Akdeniz University Faculty of Medicine, Antalya, Türkiye; [5]Department of Medical Oncology, Akdeniz University Faculty of Medicine, Antalya, Türkiye.

*Correspondence to İmren Mutlu: mutluimren4@gmail.com

DOI: 10.17305/bb.2026.14598

© 2026 Ozan Sanhal et al. This article is available under a Creative Commons License (Attribution 4.0 International, as described at https://creativecommons.org/licenses/by/4.0/).

standard mammography and digital breast tomosynthesis. Emerging evidence suggests its performance for staging and response assessment may approach that of DCE-MRI in selected settings [8–10]. Nevertheless, reported accuracy varies across studies, and direct comparisons using uniform endpoints, such as pCR, remain limited.

Fluorine-18 fluorodeoxyglucose positron emission tomography–computed tomography (^{18}F-FDG PET/CT) offers a functional assessment of tumor metabolism and has been used to evaluate treatment response in breast cancer, including during or after NAC [11]. While metabolic changes can precede anatomic changes, the ability of ^{18}F-FDG PET/CT to predict pCR and characterize residual local disease has shown variable results.

Therefore, this retrospective study aimed to compare CEM, DCE-MRI, and ^{18}F-FDG PET/CT for predicting pCR and assessing residual disease after NAC in breast cancer patients, using postoperative histopathology as the gold standard.

Materials and methods

Study design and patient population

This retrospective study adhered to the principles of the Declaration of Helsinki and was approved by the Akdeniz University Ethics Committee on March 27, 2025 (TBAEK-308), with a waiver for informed consent.

We retrospectively screened 167 consecutive breast cancer patients who underwent NAC followed by surgery at our institution between July 2023 and March 2026. In our clinical practice, NAC response is routinely assessed using CEM and ^{18}F-FDG PET/CT. However, combined assessment with CEM, DCE-MRI, and ^{18}F-FDG PET/CT was not routinely performed in all patients. DCE-MRI was obtained selectively when clinically indicated, such as in patients with suspicious symptoms, suspicious or discordant conventional imaging findings, or when detailed evaluation of local tumor extent was required. Consequently, the study cohort comprised a selected subgroup of patients who underwent all three imaging modalities for NAC response assessment. Among the 167 screened patients, 89 underwent complete post-NAC assessment with CEM, DCE-MRI, and ^{18}F-FDG PET/CT and were considered for inclusion.

Patients were excluded for pregnancy or lactation ($n = 1$), lesions outside the field of view ($n = 1$), poor image quality ($n = 2$), incomplete NAC regimen ($n = 1$), missing postoperative pathological evaluation ($n = 3$), or requirement for re-excision that prevented reliable assessment of residual tumor size or treatment response ($n = 5$). Eligible patients had complete paired pre- and post-NAC CEM, DCE-MRI, and ^{18}F-FDG PET/CT examinations, completed NAC followed by surgery, and available postoperative pathological results. This yielded 76 patients for the final analysis. The patient selection process is illustrated in Figure 1.

For each patient, the dates of CEM, DCE-MRI, and ^{18}F-FDG PET/CT were recorded separately. Baseline imaging occurred before NAC, and post-treatment imaging was performed after NAC but before surgery. No systemic therapy was administered before baseline imaging or between post-treatment imaging and surgery. Treatment plans were determined by a multidisciplinary team. Standard NAC regimens typically included anthracycline- and taxane-based therapies, with trastuzumab added for human epidermal growth factor receptor 2 (HER2)-enriched tumors. After NAC, patients underwent either BCS or mastectomy.

CEM protocol

CEM examinations were performed using a dual-energy mammography system (Giotto Class; IMS Giotto, Sagittario, Sasso Marconi, Bologna, Italy). Prior to imaging, iohexol (Omnipaque 350 mgI/mL; GE, Shanghai, China) was administered intravenously at a dose of 1.5 mL/kg using a power injector at 3 mL/s. Approximately 2 min after contrast injection, LE and high-energy (HE) craniocaudal and mediolateral oblique views were acquired sequentially, starting with the suspicious breast. RC were generated by subtracting LE from HE images. The total examination time was ≤10 min. Tube voltage was automatically adjusted based on breast thickness and density using automatic exposure control (26–31 kVp for LE exposures; 45–49 kVp for HE exposures).

DCE-MRI protocol

MRI examinations were conducted using a 1.5T MRI system (Magnetom Sola, Siemens) with a dedicated breast coil. The imaging protocol included a standard T2-weighted axial sequence with fat suppression, a T1-weighted axial sequence, axial diffusion-weighted imaging (DWI) echo-planar sequences, and apparent diffusion coefficient (ADC) maps. For DCE-MRI, a pre-contrast acquisition was followed by five post-contrast acquisitions obtained at 60-second intervals. The contrast agent, gadobutrol (0.1 mmol/kg; Gadavist, Bayer HealthCare), was administered as an intravenous bolus using a power injector at 2 mL/s, followed by a saline flush. The total dynamic acquisition time was approximately 5 min.

^{18}F-FDG PET/CT protocol

Patients fasted for at least 6 h and had serum glucose levels below 150 mg/dL before receiving 3.7 MBq/kg of ^{18}F-FDG intravenously. After a one-hour uptake period, a PET/CT scan was conducted using the Biograph 16 Horizon 3R (Siemens). Patients were positioned with arms raised, and a non-contrast CT scan was performed in the craniocaudal direction with a slice thickness of 4 mm, from the vertex to the upper thigh. PET imaging followed in the same direction and slice intervals. The acquired images were reconstructed and fused to create combined images for enhanced diagnostic evaluation.

Image analysis

All CEM and DCE-MRI images were reviewed in consensus by two breast radiologists with 15 and 5 years of experience, respectively, using a dedicated workstation. Readers were blinded to the final pathological results and to the findings of other imaging modalities. The reading order of CEM and DCE-MRI examinations was randomized.

For CEM, tumor measurements were performed on recombined images. For DCE-MRI, measurements were performed on subtracted post-contrast images. After NAC treatment,

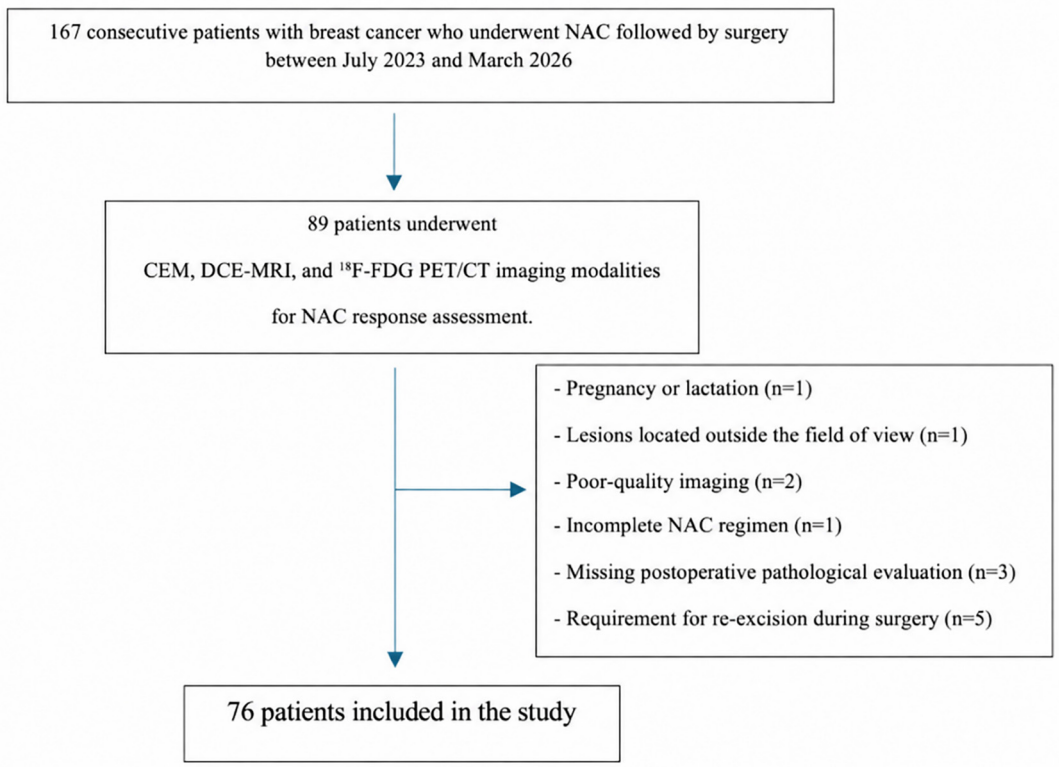


Figure 1. **Flowchart of study participant enrollment.**

residual enhancement at the primary tumor site indicated residual disease. If residual enhancement was present, the largest diameter of the enhancing lesion was recorded [12]. If no enhancing lesion was detected, the lesion size was recorded as 0 mm, and the case was classified as a radiologic complete response. Non-enhanced persistent microcalcifications on CEM were recorded separately but were not considered evidence of residual invasive disease; thus, these cases were classified as a complete response. In multifocal disease, the sum of the longest diameters of all measurable enhancing lesions was used. Multicentric lesions were measured and reported separately. Axillary lymph nodes were not evaluated; therefore, response assessment was limited to the primary breast tumor.

^{18}F-FDG PET/CT images were interpreted by a nuclear medicine specialist with 12 years of experience, who was blinded to the final pathological results as well as to CEM and DCE-MRI findings. ^{18}F-FDG PET/CT response was assessed based on abnormal FDG uptake at the primary tumor site and classified as either residual disease or metabolic complete response [13]. Metabolic complete response was defined as the resolution of abnormal FDG uptake to background levels, with no new suspicious FDG-avid lesions. Persistent focal FDG uptake above background levels at the primary tumor site was considered residual disease. Due to the limited spatial resolution of PET/CT, size-based measurements were not included in the response assessment [13, 14].

Histopathologic evaluation

All surgical specimens were reviewed by an experienced breast pathologist blinded to imaging findings. The post-NAC surgical specimen served as the reference standard for treatment response in the breast. Because axillary nodal status was not included, the primary endpoint was breast pathological complete response (breast pCR), not overall pCR.

Tumor beds were evaluated using hematoxylin-and-eosin–stained sections. When residual invasive carcinoma was present, the maximum invasive tumor diameter was recorded. For multifocal disease, the sum of the largest dimensions of each invasive focus was calculated. In multicentric disease, each tumor size was measured separately. If no residual invasive carcinoma was identified, tumor size was recorded as 0 mm. Breast pCR was defined as the absence of residual invasive carcinoma in the breast, regardless of the presence or absence of residual ductal carcinoma *in situ* (DCIS).

Statistical analysis

All analyses were performed using IBM SPSS Statistics version 23.0 (IBM Corp., Armonk, NY, USA) and JAMOVI version 2.7.18. Normality of continuous variables was assessed using the Shapiro–Wilk test and visual inspection of histograms and quantile–quantile (Q–Q) plots. Normally distributed continuous variables were reported as mean ± standard deviation (minimum–maximum), while categorical variables were summarized as frequencies and percentages.

Postoperative pathological response was accepted as the reference standard. Agreement between pathological response and imaging-based categorical responses from CEM, DCE-MRI, and ^{18}F-FDG PET/CT was evaluated using Cohen's kappa coefficient. The diagnostic performance of each imaging

Table 1. Patient and tumor characteristics

Characteristic	Value ($n = 76$)
Age (years)	
Mean ± SD (range)	50.86 ± 11.27 (26–76)
Histologic subtypes	
Invasive ductal carcinoma	63 (82.9%)
Invasive lobular carcinoma	6 (7.9%)
Rare types	7 (9.2%)
Molecular subtypes	
Luminal A	15 (19.7%)
Luminal B	33 (43.4%)
HER2-enriched	13 (17.1%)
Triple-negative breast cancer	15 (19.7%)
Focality	
Unifocal	44 (57.9%)
Multifocal	23 (30.3%)
Multicentric	9 (11.8%)
Type of surgery	
Breast-conserving surgery	40 (52.6%)
Mastectomy	36 (47.4%)

Abbreviations: HER2, human epidermal growth factor receptor 2; SD, standard deviation.

modality for predicting pCR was assessed by calculating sensitivity, specificity, positive predictive value (PPV), negative predictive value (NPV), and accuracy, with 95% confidence intervals (95% CI). Differences among modalities were compared using Cochran's Q test. When appropriate, pairwise comparisons were performed using McNemar tests with Holm-Bonferroni correction for multiple comparisons. Receiver Operating Characteristic (ROC) curve analysis evaluated the predictive performance of imaging modalities for pCR. Area under the curve (AUC) values with 95% CI were calculated, and optimal cutoff values were determined using the Youden index.

Pathological response rates among molecular subtypes were compared using Fisher's exact test with Monte Carlo simulation, and pairwise comparisons were performed using the Z-test with Bonferroni correction.

In patients with pathologically confirmed residual disease ($n = 48$), agreement between residual tumor size measured by CEM or DCE-MRI and pathology was assessed using the intraclass correlation coefficient (ICC), Bland–Altman analysis, and paired t-tests. The ICC was calculated using a two-way mixed-effects model for absolute agreement based on single measurements. For Bland–Altman analysis, the difference was defined as pathological tumor size minus imaging-based residual tumor size; mean bias and 95% limits of agreement (LOA) were calculated. A P value < 0.05 was considered statistically significant.

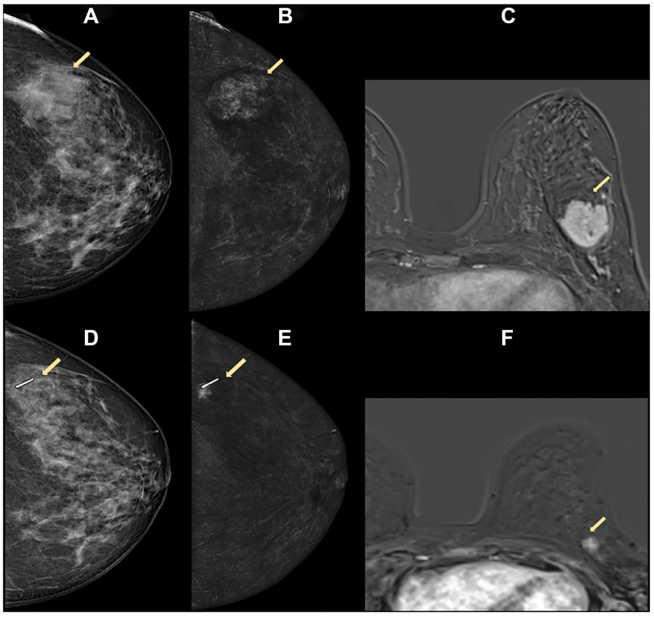


Figure 2. Residual invasive disease after neoadjuvant chemotherapy in luminal A breast cancer. A 47-year-old woman with invasive ductal carcinoma of the left breast showed a partial pathological response to NAC. (A, B) Pre-NAC low-energy and recombined CC CEM images, respectively, demonstrate the breast mass and its associated enhancement. (C) Pre-NAC axial post-contrast subtraction DCE-MRI image shows the corresponding enhancing mass. (D, E) Post-NAC low-energy and recombined CC CEM images, respectively, demonstrate the residual lesion, measuring 12 mm on the recombined image. (F) Post-NAC axial post-contrast subtraction DCE-MRI image shows a 13-mm residual enhancing mass. Yellow arrows indicate the lesion before and after treatment. ^{18}F-FDG PET/CT (not shown) demonstrated a decrease in SUVmax from 16 before NAC to 4.1 after NAC, with persistent metabolic activity in the residual lesion. Histopathological examination following BCS confirmed 12 mm of residual invasive carcinoma. **Abbreviations**: BCS, breast-conserving surgery; CC, craniocaudal; CEM, contrast-enhanced mammography; DCE-MRI, dynamic contrast-enhanced magnetic resonance imaging; ^{18}F-FDG PET/CT, fluorine-18 fluorodeoxyglucose positron emission tomography/computed tomography; NAC, neoadjuvant chemotherapy; SUVmax, maximum standardized uptake value.

Results

Patient and tumor characteristics

This retrospective study included 76 patients with a mean age of 50.86 ± 11.27 years (range, 26–76 years). Histologically, 63 tumors (82.9%) were invasive ductal carcinoma, 6 (7.9%) were invasive lobular carcinoma, and 7 (9.2%) were rare histologic variants. Molecular subtypes included luminal A in 15 patients (19.7%), luminal B in 33 (43.4%), HER2-enriched in 13 (17.1%), and triple-negative breast cancer (TNBC) in 15 (19.7%). Multifocal disease was present in 23 (30.3%) patients, and multicentric disease in 9 (11.8%) patients. Baseline characteristics are summarized in Table 1.

At diagnosis, CEM, DCE-MRI, and ^{18}F-FDG PET/CT were performed within a mean interval of 19 days (range, 6–44 days). Response assessment after NAC was performed a mean of 11 days after treatment completion (range, 5–31 days). The mean interval between post-NAC imaging and surgery was 9 days

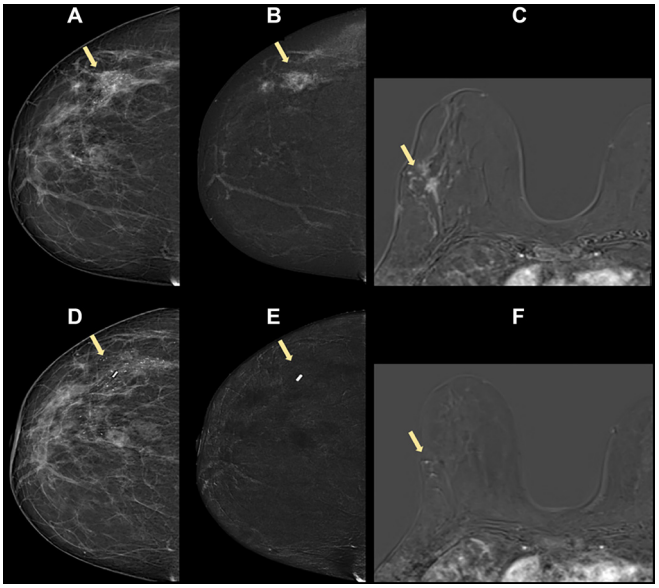


Figure 3. Pathologic complete response after neoadjuvant chemotherapy in HER2-enriched breast cancer. A 55-year-old woman with invasive ductal carcinoma of the right breast achieved a pathologic complete response after NAC. (A, B) Pre-NAC low-energy and recombined CC CEM images, respectively, show the index lesion as a mass with associated enhancement; microcalcifications are also present on the low-energy image. (C) Pre-NAC axial post-contrast subtraction DCE-MRI image demonstrates the corresponding enhancing lesion with associated non-mass enhancement. (D) Post-NAC low-energy CC CEM image shows persistent residual microcalcifications despite treatment response. (E) Post-NAC recombined CC CEM image shows no residual abnormal enhancement at the tumor site. (F) Post-NAC axial post-contrast subtraction DCE-MRI image likewise demonstrates no residual enhancing lesion. Yellow arrows indicate the tumor site, and white arrows indicate residual microcalcifications. ^{18}F-FDG PET/CT (not shown) demonstrated complete metabolic response, with disappearance of the previously increased uptake (pre-NAC SUVmax 4.3). Histopathological examination after mastectomy confirmed pathologic complete response. **Abbreviations**: CC, craniocaudal; CEM, contrast-enhanced mammography; DCE-MRI, dynamic contrast-enhanced magnetic resonance imaging; ^{18}F-FDG PET/CT, fluorine-18 fluorodeoxyglucose positron emission tomography/computed tomography; HER2, human epidermal growth factor receptor 2; NAC, neoadjuvant chemotherapy; SUVmax, maximum standardized uptake value.

(range, 3–27 days). BCS was performed in 40 (52.6%) patients, and mastectomy in 36 (47.4%) patients.

Prediction of pCR

According to postoperative pathological assessment, pCR was achieved in 28 (36.8%) patients, while residual disease was present in 48 (63.2%) patients. pCR rates differed significantly among molecular subtypes ($P = 0.021$). The highest pCR rate was observed in the HER2-enriched group (69.2%), followed by TNBC (40.0%), luminal B (33.3%), and luminal A (13.3%). In pairwise comparisons, only the difference between luminal A and HER2-enriched tumors was significant. Representative cases demonstrating residual disease and complete response after NAC are shown in Figures 2 and 3.

The diagnostic performance of CEM, DCE-MRI, and ^{18}F-FDG PET/CT is shown in Table 2. All three modalities demonstrated significant moderate agreement with pathological response. The highest agreement was observed for CEM ($\kappa = 0.579$, $P < 0.001$), followed by DCE-MRI ($\kappa = 0.475$, $P < 0.001$) and ^{18}F-FDG PET/CT ($\kappa = 0.451$, $P < 0.001$).

CEM showed the highest sensitivity, NPV, and accuracy for predicting pCR, with a sensitivity of 89.3%, specificity of 72.9%, PPV 65.8%, NPV of 92.1%, and accuracy of 79.0%. DCE-MRI showed the highest specificity and PPV, with a sensitivity of 60.7%, specificity of 85.4%, PPV of 70.8%, NPV of 78.8%, and accuracy of 76.3%. ^{18}F-FDG PET/CT demonstrated a sensitivity of 71.4%, specificity of 75.0%, PPV of 62.5%, NPV of 81.8%, and accuracy of 73.7%.

In pairwise comparisons, overall diagnostic accuracy did not differ significantly among the three modalities ($P = 0.661$). However, sensitivity differed significantly, with CEM showing higher sensitivity than DCE-MRI ($P = 0.012$). Although DCE-MRI had the highest specificity, this difference was not statistically significant ($P = 0.179$).

The accuracy of CEM, DCE-MRI, and ^{18}F-FDG PET/CT for predicting pCR was higher in unifocal lesions than in multifocal or multicentric lesions; however, these differences were not statistically significant for any modality ($P = 0.094$, $P = 0.358$, and $P = 0.921$, respectively).

ROC analysis also showed significant predictive performance for all modalities (Figure 4). DCE-MRI achieved the highest AUC, although it was very similar to that of CEM (0.844 vs. 0.841, respectively), whereas ^{18}F-FDG PET/CT showed a lower AUC of 0.769; all AUC values were statistically significant ($P < 0.001$).

Non-enhancing microcalcifications were detected on CEM in 12 patients. CEM indicated complete response in all 12 cases, compared with 6 (50.0%) on DCE-MRI and 8 (66.7%) on ^{18}F-FDG PET/CT. Surgical pathology confirmed complete response in 11 of these patients: 8 patients had pCR and 3 had residual DCIS. One patient had an 8-mm residual invasive tumor.

In three patients, CEM showed non-enhancing masses and ^{18}F-FDG PET/CT indicated complete metabolic response. Further morphological assessment with DCE-MRI suggested necrosis, hemorrhagic cyst formation, and fibrosis, respectively. However, pathology revealed small residual invasive tumors measuring 2 mm, 6 mm, and 7 mm, respectively.

Tumor size assessment after NAC

Among the 48 patients with residual disease on pathology, the mean residual invasive tumor size was 18.19 ± 17.83 mm (range, 2–92 mm). The mean residual invasive tumor size measured on post-NAC CEM was 22.69 ± 24.14 mm (range, 0–103 mm), while the corresponding mean invasive tumor size on DCE-MRI was 22.35 ± 21.23 mm (range, 0–89 mm).

Agreement between imaging-based and pathological tumor size measurements is presented in Table 3 and Figure 5. Bland–Altman differences were calculated as pathological size minus imaging-based size; therefore, negative values indicate imaging overestimation. Both imaging modalities slightly overestimated residual tumor size compared with pathology. The mean bias was −4.50 mm for CEM, with LOA from −34.16 to 25.16 mm, and −4.17 mm for DCE-MRI, with LOA from −29.26 to

Table 2. Performance of imaging modalities for detecting pCR following NAC

	Pathology		Kappa (κ)	P	Sensitivity (%) (95% CI)	Specificity (%) (95% CI)	PPV (%) (95% CI)	NPV (%) (95% CI)	Accuracy (%) (95% CI)	AUC (95% CI)
	Residual disease	pCR								
CEM response										0.841 (0.767–0.915)
Residue	35 (72.9)	3 (10.7)								
rCR	13 (27.1)	25 (89.3)	0.579	< **0.001**	89.3 (71.77–97.73)	72.9 (58.15–84.72)	65.8 (54.30–75.69)	92.1 (79.80–97.18)	79.0 (68.08–87.46)	
DCE-MRI response										0.844 (0.758–0.929)
Residue	41 (85.4)	11 (39.3)								
rCR	7 (14.6)	17 (60.7)	0.475	< **0.001**	60.7 (40.58–78.50)	85.4 (72.24–93.93)	70.8 (53.51–83.67)	78.8 (69.86–85.70)	76.3 (65.18–85.32)	
^{18}F-FDG PET/CT response										0.769 (0.671–0.867)
Residue	36 (75.0)	8 (28.6)								
mCR	12 (25.0)	20 (71.4)	0.451	< **0.001**	71.4 (51.33–86.78)	75.0 (60.40–86.36)	62.5 (49.19–74.15)	81.8 (71.01–89.21)	73.7 (62.32–83.13)	

Abbreviations: AUC, area under the curve; CEM, contrast-enhanced mammography; CI, confidence interval; DCE-MRI, dynamic contrast-enhanced magnetic resonance imaging; ^{18}F-FDG PET/CT, fluorine-18 fluorodeoxyglucose positron emission tomography/computed tomography; mCR, metabolic complete response; NPV, negative predictive value; pCR, pathologic complete response; PPV, positive predictive value; rCR, radiologic complete response.

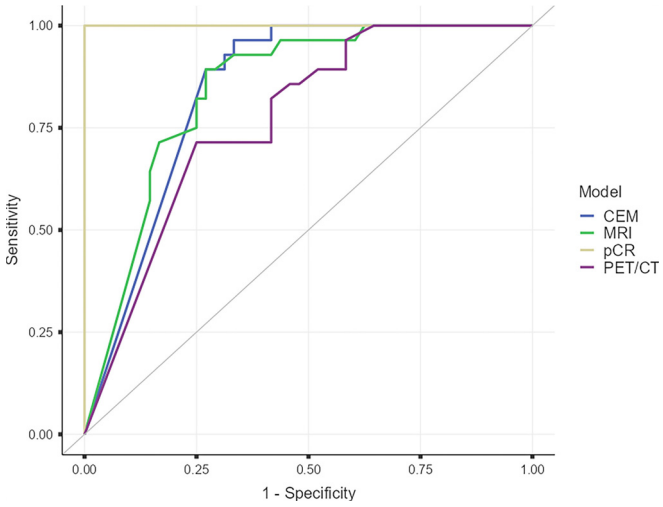


Figure 4. Receiver operating characteristic curves for predicting breast pathologic complete response after neoadjuvant chemotherapy. ROC curves show the predictive performance of CEM (blue), DCE-MRI (green), and ^{18}F-FDG PET/CT (purple), using postoperative histopathology as the reference standard for breast pCR. The AUC values were 0.841 (95% CI: 0.767–0.915) for CEM, 0.844 (95% CI: 0.758–0.929) for DCE-MRI, and 0.769 (95% CI: 0.671–0.867) for ^{18}F-FDG PET/CT. Sensitivity is plotted against 1 - specificity, and the gray diagonal line indicates no discrimination (AUC = 0.5). **Abbreviations**: AUC, area under the curve; CEM, contrast-enhanced mammography; CI, confidence interval; DCE-MRI, dynamic contrast-enhanced magnetic resonance imaging; ^{18}F-FDG PET/CT, fluorine-18 fluorodeoxyglucose positron emission tomography/computed tomography; pCR, pathologic complete response; ROC, receiver operating characteristic.

20.93 mm. ICC analysis showed good agreement with pathology for both imaging modalities, with ICC values of 0.733 (95% CI: 0.565–0.842) for CEM and 0.773 (95% CI: 0.620–0.868) for DCE-MRI, both $P < 0.001$.

Discussion

Accurate evaluation of pCR and residual disease following NAC is crucial for surgical planning and prognostic assessment in breast cancer. This study directly compared CEM, DCE-MRI, and ^{18}F-FDG PET/CT within the same patient cohort, using postoperative histopathology as the reference standard. While each of these imaging modalities has been previously investigated, direct intra-patient comparisons involving all three techniques are uncommon in the literature. Most available studies have focused on paired comparisons, typically CEM vs DCE-MRI or DCE-MRI vs ^{18}F-FDG PET/CT. A key strength of the present study is that all patients underwent CEM, DCE-MRI, and ^{18}F-FDG PET/CT both before and after NAC. This enabled a true within-subject comparison of treatment response across modalities, reducing interpatient variability and providing clinically relevant evidence for selecting the most appropriate imaging technique for post-NAC assessment. Importantly, our analysis addresses a clinically actionable question: which modality, or combination of modalities, most reliably predicts NAC treatment response in routine practice? The findings may help guide imaging modality selection, particularly in centers where any modality is unavailable, contraindicated, or poorly

Table 3. Comparison of imaging modalities and pathologic tumor size

Imaging modality ($n = 48$)	Mean difference (bias), mm	LOA (mm)	Concordance, ICC (95% CI)	*P*
CEM	−4.50	−34.16 to 25.16	0.733 (0.565–0.842)	< 0.001
DCE-MRI	−4.17	−29.26 to 20.93	0.773 (0.620–0.868)	< 0.001

Abbreviations: CEM, contrast-enhanced mammography; CI, confidence interval; DCE-MRI, dynamic contrast-enhanced magnetic resonance imaging; ICC, intraclass correlation coefficient; LOA, limits of agreement.

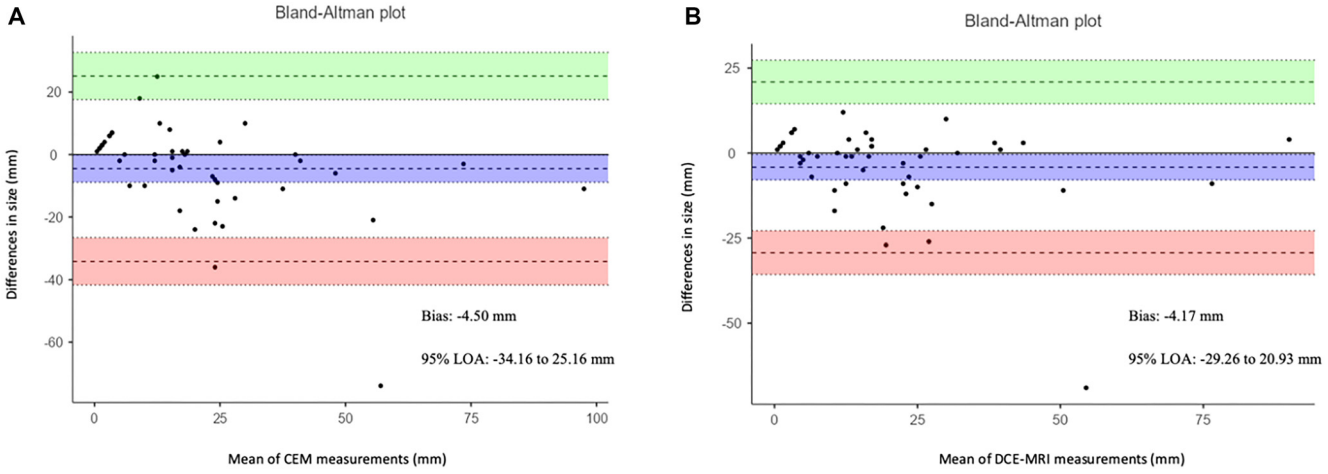


Figure 5. Bland–Altman agreement between imaging-based and pathological residual tumor size after neoadjuvant chemotherapy. Plots compare residual tumor size measured by (A) CEM and (B) DCE-MRI with postoperative pathological measurements in 48 patients with residual invasive disease. Each point represents one patient. The vertical axis shows pathological tumor size minus imaging-based tumor size; negative values therefore indicate imaging overestimation. The central dashed line within the blue band represents the mean difference (bias), whereas the upper and lower dashed lines within the green and red bands indicate the 95% LOA, respectively. The solid horizontal line marks zero difference. Mean bias was −4.50 mm for CEM, with 95% LOA of −34.16 to 25.16 mm, and −4.17 mm for DCE-MRI, with 95% LOA of −29.26 to 20.93 mm. **Abbreviations**: CEM, contrast-enhanced mammography; DCE-MRI, dynamic contrast-enhanced magnetic resonance imaging; LOA, limits of agreement.

tolerated, and may provide a foundation for future prospective multicenter validation.

In this retrospective study, CEM, DCE-MRI, and ^{18}F-FDG PET/CT all demonstrated significant agreement with postoperative pathological response after NAC in patients with breast cancer. The pCR rate of 36.8% in our cohort aligns with expected response rates in mixed breast cancer populations. As anticipated, pCR varied substantially by molecular subtype, with HER2-enriched tumors exhibiting the highest response rates, followed by TNBC, while luminal A tumors demonstrated the lowest response. This pattern reflects the known superior chemosensitivity of HER2-enriched and TNBC tumors compared with hormone receptor-positive, low-proliferative cancers [15].

Overall, no significant difference in diagnostic accuracy was detected among the three modalities in this exploratory retrospective cohort, although each technique demonstrated different diagnostic strengths. CEM demonstrated the highest sensitivity (89.3%), NPV (92.1%), and accuracy (79.0%) for predicting pCR. These findings suggest that CEM may be useful for identifying patients with a marked response to NAC treatment and for reducing the risk of underestimating residual disease. Its high NPV indicates that when CEM suggests residual disease, true residual disease is likely, which is clinically important in response-adaptive treatment strategies. On the other hand, DCE-MRI showed the highest specificity (85.4%), PPV (70.8%), and AUC (0.844), indicating a more conservative and reliable assessment of pCR. This may help reduce false-positive classifications of complete response and supports the continued role of DCE-MRI as a reference imaging modality after NAC. Although DCE-MRI demonstrated slightly better specificity, the AUC values of DCE-MRI and CEM were very similar in this cohort (0.844 vs. 0.841). However, given the retrospective design and the absence of a formal equivalence analysis, these findings should not be interpreted as demonstrating equivalence or interchangeability between CEM and DCE-MRI.

These results are consistent with previous studies reporting good agreement between CEM and DCE-MRI, although their relative performance has varied across reports [16–23]. Wang et al. reported slightly higher accuracy (0.86 vs. 0.75) and specificity (94% vs. 71%) for DCE-MRI compared with CEM in predicting pCR [16]. Hogan et al. found that DCE-MRI showed higher sensitivity (88% vs. 81%), NPV (60% vs. 50%), and accuracy (77% vs. 72%) than CEM, but lower specificity (47% vs. 50%), while PPV was similar for both modalities (81% vs. 81%) [17]. In contrast, a meta-analysis by Kaiyin et al. reported that

CEM had higher sensitivity than DCE-MRI (93% vs. 84%) but lower specificity (68% vs. 80%) for pCR prediction [18]. These differences may reflect variations in study design, patient populations, tumor subtypes, imaging protocols, interpretation criteria, and definitions of treatment response. In the present study, CEM showed no significant difference in diagnostic performance compared to DCE-MRI in selected patients. Rather than establishing CEM as a replacement for DCE-MRI, our results suggest that CEM may be considered as a potential imaging option in selected clinical settings, particularly when MRI is unavailable, contraindicated, or poorly tolerated.

^{18}F-FDG PET/CT showed moderate agreement with postoperative pathology and acceptable diagnostic performance; however, it appeared less reliable than CEM and DCE-MRI for assessing local residual disease. Previous studies comparing DCE-MRI and ^{18}F-FDG PET/CT have reported variable results. An YY et al. reported comparable sensitivity between the two modalities, but higher specificity and accuracy for DCE-MRI [24]. The meta-analysis by Caracciolo et al. demonstrated substantial heterogeneity among studies, which was partly attributed to differences in tumor molecular subtype and primary tumor volume [14]. Some reports suggest ^{18}F-FDG PET/CT may offer greater specificity, while DCE-MRI provides greater sensitivity in assessing pCR.

Direct comparisons between CEM and ^{18}F-FDG PET/CT for pCR assessment remain limited. In our cohort, CEM and ^{18}F-FDG PET/CT showed no statistically significant differences in sensitivity (89.3% vs. 71.4%) or specificity (72.9% vs. 75.0%). However, CEM showed a higher NPV (92.1% vs. 81.8%), suggesting greater reliability in identifying patients with residual invasive disease. In addition, ^{18}F-FDG PET/CT showed lower concordance with pathological response ($\kappa = 0.451$). This may be attributable to its limited spatial resolution and reduced sensitivity for detecting small-volume residual disease, residual DCIS, low-grade tumors, or lesions with low glycolytic activity.

These findings suggest that ^{18}F-FDG PET/CT should not be used as a standalone imaging modality for local response assessment after NAC. However, it remains clinically valuable for systemic staging, detection of distant metastases, and evaluation of whole-body treatment response. Therefore, in the post-NAC setting, ^{18}F-FDG PET/CT should be regarded as complementary to breast-directed imaging modalities such as CEM and DCE-MRI, which remain more suitable for local assessment of residual breast disease.

For residual invasive tumor size assessment, both CEM and DCE-MRI demonstrated strong agreement with pathological tumor measurements, with ICC values of 0.733 and 0.773, respectively, indicating good reproducibility. Bland–Altman analysis revealed small systematic biases for both modalities (−4.50 mm for CEM and −4.17 mm for DCE-MRI), which are clinically negligible considering the precision limits of surgical pathology measurements and the inherent variability in tumor sectioning protocols. These minimal biases suggest that either modality systematically over- or underestimates residual disease burden. However, the relatively wide LOA (CEM: −34.16 to 25.16 mm; DCE-MRI: −29.26 to 20.93 mm) indicate that individual-level discrepancies may exceed 3 cm. Therefore, although both modalities provide broadly comparable estimates of residual tumor burden, they may not be reliably interchangeable for individual patients. This is particularly relevant in borderline cases, where inaccurate tumor size estimation could influence surgical planning, postoperative risk stratification, and adjuvant treatment decisions. Accordingly, imaging-based size estimates that fall close to clinically relevant thresholds should be interpreted cautiously and in conjunction with other imaging information. These results are consistent with previous studies reporting variable radiologic–pathologic concordance [19–23], including the findings of Fallenberg et al., who observed that discrepancies tend to increase in larger residual tumors [21].

An important finding was the limited reliability of enhancement-based imaging in the presence of residual microcalcifications. In 12 patients, non-enhancing microcalcifications persisted on CEM despite imaging suggesting a complete response. Although most of these cases lacked residual invasive tumor in postoperative pathological assessment, three patients showed residual DCIS and one had an 8-mm residual invasive tumor at pathology. Because DCIS may show little to no enhancement or FDG uptake, residual calcifications should be carefully evaluated on LE CEM images and correlated with pretreatment mammography findings and lesion morphology. Their presence should still be considered during surgical planning [25, 26].

Minimal residual disease also proved challenging to detect in several cases. Small residual invasive tumors, only a few millimeters in size, were missed or interpreted as post-treatment changes like fibrosis, necrosis, hemorrhagic cyst formation, or complete response. These findings highlight the difficulty of detecting small-volume viable tumors after NAC, especially when residual disease exhibits low vascularity or limited metabolic activity.

Treatment-related changes after NAC may explain both false-positive and false-negative imaging findings. Inflammation in the tumor can cause persistent enhancement, leading to an overestimation of residual disease. Conversely, fibrosis, necrosis, reduced vascularity, and other regressive changes may mask viable tumor cells, leading to an underestimation of disease [27, 28]. Imaging–pathology agreement may also vary with tumor biology; TNBC and HER2-enriched tumors generally show better radiologic–pathologic correlation than hormone receptor-positive tumors [29, 30]. Although post-NAC imaging was performed before surgery in all patients, the interval between imaging and pathological assessment varied. Continued treatment-related changes in the tumor bed, including fibrosis, necrosis, inflammation, or residual tumor regression/progression, may have occurred during this interval, contributing to imaging-pathology discordance. This variability should therefore be considered when interpreting the accuracy of imaging-based response assessment.

This study has several limitations. First, its retrospective, single-center design and relatively small sample size limit the generalizability of the findings and reduce statistical power. Second, selection bias may have occurred because only patients who underwent all three imaging modalities were included. At our institution, CEM and ^{18}F-FDG PET/CT are routinely

used after NAC, whereas DCE-MRI is performed selectively for suspicious symptoms, discordant imaging findings, or more detailed assessment of local tumor extent. Therefore, the cohort may represent more complex cases rather than an unselected NAC population, potentially affecting the reported diagnostic accuracy estimates. Third, imaging was performed as part of routine clinical care rather than a standardized protocol, resulting in variable examination timing. Consequently, interval changes in tumor burden between imaging studies, or between imaging and pathological assessment, cannot be excluded. Fourth, the present analysis focused primarily on the diagnostic performance of CEM, DCE-MRI, and ^{18}F-FDG PET/CT for predicting pCR and estimating residual invasive tumor size. Therefore, subgroup analyses by molecular subtype, tumor grade, clinical stage, and NAC regimen were not performed. Fifth, axillary nodal response was not evaluated because the axilla was not consistently included in the imaging field of view. Sixth, interobserver agreement between the two radiologists was not evaluated. Finally, quantitative ^{18}F-FDG PET/CT parameters such as maximum standardized uptake value (SUVmax) and MRI parameters such as DWI, ADC values, and detailed lesion morphology were not included in the final analysis. Pathological measurement was also based on the longest diameter of the invasive component, which may not fully represent scattered, multifocal, or heterogeneous residual tumor burden after NAC. These factors should be considered when interpreting imaging-based predictions of complete response and residual tumor size.

Conclusion

In conclusion, in this exploratory retrospective cohort, CEM, DCE-MRI, and ^{18}F-FDG PET/CT showed potential for assessing treatment response after NAC in breast cancer patients. In our dataset, CEM demonstrated higher sensitivity, NPV, and accuracy for predicting pCR, whereas DCE-MRI showed higher specificity, PPV, and AUC. No significant difference in overall diagnostic accuracy was detected between CEM and DCE-MRI in this cohort. CEM and DCE-MRI also showed strong agreement with pathological residual tumor size. ^{18}F-FDG PET/CT provided metabolic response information; however, its performance for local residual disease assessment appeared more limited, particularly in small-volume residual tumors, residual DCIS, and lesions associated with microcalcifications.

Although CEM showed promising results in this selected cohort, no definitive conclusion can be drawn regarding its superiority, equivalence, or interchangeability with DCE-MRI or ^{18}F-FDG PET/CT. Rather, these findings suggest that CEM may represent a potentially useful imaging tool for post-NAC response assessment in appropriately selected patients. The results should be interpreted cautiously due to the retrospective design, selected patient population, small number of pCR cases, and absence of external validation. Further prospective, multicenter studies with larger cohorts are needed to validate these observations and clarify the roles of CEM, DCE-MRI, and ^{18}F-FDG PET/CT in post-NAC response assessment.

Conflicts of interest: Authors declare no conflicts of interest.

Funding: Authors received no specific funding for this work.

Submitted: 18 June 2026
Accepted: 17 September 2026
Published online: 28 September 2026

References

[1] Korde LA, Somerfield MR, Carey LA, Crews JR, Denduluri N, Hwang ES, et al. Neoadjuvant chemotherapy, endocrine therapy, and targeted therapy for breast cancer: ASCO guideline. J Clin Oncol 2021;39(13):1485–505. https://doi.org/10.1200/JCO.20.03399.

[2] Mamounas EP. Impact of neoadjuvant chemotherapy on locoregional surgical treatment of breast cancer. Ann Surg Oncol 2015;22(5):1425–33. https://doi.org/10.1245/s10434-015-4406-6.

[3] National Comprehensive Cancer Network. Invasive breast cancer guidelines, version 2.2016 [Internet]. [cited 2022 May 12]. Available from: https://www.nccn.org/professionals/physician/_gls/pdf/breast.pdf.

[4] Trimboli RM, Giorgi Rossi P, Battisti NML, Cozzi A, Magni V, Zanardo M, et al. Do we still need breast cancer screening in the era of targeted therapies and precision medicine? Insights Imaging 2020;11(1):105. https://doi.org/10.1186/s13244-020-00905-3.

[5] Asaoka M, Gandhi S, Ishikawa T, Takabe K. Neoadjuvant chemotherapy for breast cancer: past, present, and future. Breast Cancer (Auckl) 2020;14:1178223420980377. https://doi.org/10.1177/1178223420980377.

[6] Marinovich ML, Houssami N, Macaskill P, Sardanelli F, Irwig L, Mamounas EP, et al. Meta-analysis of magnetic resonance imaging in detecting residual breast cancer after neoadjuvant therapy. J Natl Cancer Inst 2013;105(5):321–33. https://doi.org/10.1093/jnci/djs528.

[7] Cozzi A, Schiaffino S, Sardanelli F. The emerging role of contrast-enhanced mammography. Quant Imaging Med Surg 2019;9(12):2012–8. https://doi.org/10.21037/qims.2019.11.09.

[8] Jochelson MS, Lobbes MBI. Contrast-enhanced mammography: state of the art. Radiology 2021;299(1):36–48. https://doi.org/10.1148/radiol.2021201948.

[9] Lobbes MBI, Heuts EM, Moossdorff M, van Nijnatten TJA. Contrast enhanced mammography (CEM) versus magnetic resonance imaging (MRI) for staging of breast cancer: the pro CEM perspective. Eur J Radiol 2021;142:109883. https://doi.org/10.1016/j.ejrad.2021.109883.

[10] Bernardi D, Vatteroni G, Acquaviva A, Valentini M, Sabatino V, Bolengo I, et al. Contrast-enhanced mammography versus MRI in the evaluation of neoadjuvant therapy response in patients with breast cancer: a prospective study. AJR Am J Roentgenol 2022;219(6):884–94. https://doi.org/10.2214/AJR.22.27756.

[11] Hofman MS, Hicks RJ. How we read oncologic FDG PET/CT. Cancer Imaging 2016;16(1):35. https://doi.org/10.1186/s40644-016-0091-3.

[12] Schwartz LH, Litière S, de Vries E, Ford R, Gwyther S, Mandrekar S, et al. RECIST 1.1 – update and clarification: from the RECIST committee. Eur J Cancer 2016;62:132–7. https://doi.org/10.1016/j.ejca.2016.03.081.

[13] O JH, Lodge MA, Wahl RL. Practical PERCIST: a simplified guide to PET response criteria in solid tumors 1.0. Radiology 2016;280(2):576–84. https://doi.org/10.1148/radiol.2016142043.

[14] Caracciolo M, Castello A, Urso L, Borgia F, Marzola MC, Uccelli L, et al. Comparison of MRI vs. [18F]FDG PET/CT for treatment response evaluation of primary breast cancer after neoadjuvant chemotherapy: literature review and future perspectives. J Clin Med 2023;12(16):5355. https://doi.org/10.3390/jcm12165355.

[15] Houssami N, Macaskill P, von Minckwitz G, Marinovich ML, Mamounas E. Meta-analysis of the association of breast cancer subtype and pathologic complete response to neoadjuvant chemotherapy. Eur J Cancer 2012;48(18):3342–54. https://doi.org/10.1016/j.ejca.2012.05.023.

[16] Wang S, Li J, Chen R, Li R, Shen X, Qian M, et al. Head to head comparison of contrast enhanced mammography and MRI in assessing the tumor response to neoadjuvant therapy in breast cancer: a prospective, multireader study. Radiol Med 2025;130(10):1561–74. https://doi.org/10.1007/s11547-025-02068-x.

[17] Hogan MP, Horvat JV, Ross DS, Sevilimedu V, Jochelson MS, Kirstein LJ, et al. Contrast-enhanced mammography in the assessment of residual disease after neoadjuvant treatment. Breast Cancer Res Treat 2023;198(2):349–59. https://doi.org/10.1007/s10549-023-06865-8.
[18] Kaiyin M, Lingling T, Leilei T, Wenjia L, Bin J. Head-to-head comparison of contrast-enhanced mammography and contrast-enhanced MRI for assessing pathological complete response to neoadjuvant therapy in patients with breast cancer: a meta-analysis. Breast Cancer Res Treat 2023;202(1):1–9. https://doi.org/10.1007/s10549-023-07034-7.
[19] Barra FR, Sobrinho AB, Barra RR, Magalhães MT, Aguiar LR, de Albuquerque GFL, et al. Contrast-enhanced mammography (CEM) for detecting residual disease after neoadjuvant chemotherapy: a comparison with breast magnetic resonance imaging (MRI). Biomed Res Int 2018;2018:8531916. https://doi.org/10.1155/2018/8531916.
[20] Łuczyńska E, Heinze-Paluchowska S, Hendrick E, Dyczek S, Ryś J, Herman K, et al. Comparison between breast MRI and contrast-enhanced spectral mammography. Med Sci Monit 2015;21:1358–67. https://doi.org/10.12659/MSM.893018.
[21] Fallenberg EM, Dromain C, Diekmann F, Engelken F, Krohn M, Singh JM, et al. Contrast-enhanced spectral mammography versus MRI: initial results in the detection of breast cancer and assessment of tumour size. Eur Radiol 2014;24(1):256–64. https://doi.org/10.1007/s00330-013-3007-7.
[22] Patel BK, Hilal T, Covington M, Zhang N, Kosiorek HE, Lobbes M, et al. Contrast-enhanced spectral mammography is comparable to MRI in the assessment of residual breast cancer following neoadjuvant systemic therapy. Ann Surg Oncol 2018;25(5):1350–6. https://doi.org/10.1245/s10434-018-6413-x.
[23] Lobbes MB, Lalji UC, Nelemans PJ, Houben I, Smidt ML, Heuts E, et al. The quality of tumor size assessment by contrast-enhanced spectral mammography and the benefit of additional breast MRI. J Cancer 2015;6(2):144–50. https://doi.org/10.7150/jca.10705.
[24] An YY, Kim SH, Kang BJ, Lee AW. Treatment response evaluation of breast cancer after neoadjuvant chemotherapy and usefulness of the imaging parameters of MRI and PET/CT. J Korean Med Sci 2015;30(6):808–15. https://doi.org/10.3346/jkms.2015.30.6.808.
[25] An YY, Kim SH, Kang BJ. Residual microcalcifications after neoadjuvant chemotherapy for locally advanced breast cancer: comparison of the accuracies of mammography and MRI in predicting pathological residual tumor. World J Surg Oncol 2017;15(1):198. https://doi.org/10.1186/s12957-017-1263-8
[26] Elverici E, Gündoğdu S, Gunbey Karabekmez L, Kayaçetin S, Altun Özdemir B, Gökhan MB, et al. Diagnostic performance of contrast-enhanced spectral mammography in the evaluation of suspicious microcalcifications without associated mass. Acta Radiol 2025 Oct;6:2841851251380868. https://doi.org/10.1177/02841851251380868.
[27] Wasser K, Sinn HP, Fink C, Klein SK, Junkermann H, Lüdemann HP, et al. Accuracy of tumor size measurement in breast cancer using MRI is influenced by histological regression induced by neoadjuvant chemotherapy. Eur Radiol 2003;13(6):1213–23. https://doi.org/10.1007/s00330-002-1730-6.
[28] Marinovich ML, Macaskill P, Irwig L, Sardanelli F, von Minckwitz G, Mamounas E, et al. Meta-analysis of agreement between MRI and pathologic breast tumour size after neoadjuvant chemotherapy. Br J Cancer 2013;109(6):1528–36. https://doi.org/10.1038/bjc.2013.473.
[29] McGuire KP, Toro-Burguete J, Dang H, Young J, Soran A, Zuley M, et al. MRI staging after neoadjuvant chemotherapy for breast cancer: does tumor biology affect accuracy? Ann Surg Oncol 2011;18(11):3149–54. https://doi.org/10.1245/s10434-011-1912-z.
[30] De Los Santos JF, Cantor A, Amos KD, Forero A, Golshan M, Horton JK, et al. Magnetic resonance imaging as a predictor of pathologic response in patients treated with neoadjuvant systemic treatment for operable breast cancer. Translational Breast Cancer Research Consortium trial 017. Cancer 2013;119(10):1776–83. https://doi.org/10.1002/cncr.27995.

Related articles

1. The value of 18F-FDG PET/CT imaging in breast cancer staging

Ulkem Yararbas et al., BJBMS, 2018

2. Deep learning predicts HER2 status in invasive breast cancer from multimodal ultrasound and MRI

Yuhong Fan et al., Biomol Biomed, 2025